

Recovering the systemic redshift of galaxies from their Lyman-alpha line profile

A. Verhamme^{1,2*}, T. Garel¹, E. Ventou³, T. Contini³, N. Bouché³, E.C. Herenz¹⁴, J. Richard¹, R. Bacon¹, K.B. Schmidt⁴, M. Maseda⁵, R.A. Marino⁷, J. Brinchmann^{5,6}, S. Cantalupo⁷, J. Caruana^{8,9}, B. Clément¹, C. Diener^{13,4}, A.B. Drake¹, T. Hashimoto^{1,10,11}, H. Inami¹, J. Kerutt⁴, W. Kollatschny¹², F. Leclercq¹, V. Patrício¹, J. Schaye⁵, L. Wisotzki⁴, J. Zabl³

¹ Univ Lyon, Univ Lyon1, Ens de Lyon, CNRS, Centre de Recherche Astrophysique de Lyon UMR5574, F-69230, Saint-Genis-Laval, France

² Observatoire de Genève, Université de Genève, 51 Ch. des Maillettes, 1290 Versoix, Switzerland

³ Institut de Recherche en Astrophysique et Planétologie (IRAP), Université de Toulouse, CNRS, UPS, F-31400 Toulouse, France

⁴ Leibniz-Institut für Astrophysik Potsdam (AIP), An der Sternwarte 16, D-14482, Potsdam, Germany

⁵ Leiden Observatory, Leiden University, NL-2300 RA Leiden, Netherlands

⁶ Instituto de Astrofísica e Ciências do Espaço, Universidade do Porto, CAUP, Rua das Estrelas, PT4150-762 Porto, Portugal

⁷ Department of Physics, ETH Zürich, Wolfgang–Pauli–Strasse 27, 8093 Zürich, Switzerland

⁸ Department of Physics, University of Malta, Msida MSD 2080, Malta

⁹ Institute for Space Sciences and Astronomy, University of Malta, Msida MSD 2080, Malta

¹⁰ National Astronomical Observatory of Japan, 2-21-1 Osawa, Mitaka, Tokyo 181-8588, Japan

¹¹ College of General Education, Osaka Sangyo University, 3-1-1 Nakagaito, Daito, Osaka 574-8530, Japan

¹² Institut für Astrophysik, Universität Göttingen, Friedrich-Hund Platz 1, D-37077 Göttingen, Germany

¹³ Institute of Astronomy, Madingley Road Cambridge, CB3 0HA, UK

¹⁴ Department of Astronomy, Stockholm University, AlbaNova University Centre, SE-106 91, Stockholm, Sweden

Accepted XXX. Received YYY; in original form ZZZ

ABSTRACT

The Lyman alpha ($\text{Ly}\alpha$) line of Hydrogen is a prominent feature in the spectra of star-forming galaxies, usually redshifted by a few hundreds of km s^{-1} compared to the systemic redshift. This large offset hampers follow-up surveys, galaxy pair statistics and correlations with quasar absorption lines when only $\text{Ly}\alpha$ is available. We propose diagnostics that can be used to recover the systemic redshift directly from the properties of the $\text{Ly}\alpha$ line profile. We use spectroscopic observations of Lyman-Alpha Emitters (LAEs) for which a precise measurement of the systemic redshift is available. Our sample contains 13 sources detected between $z \approx 3$ and $z \approx 6$ as part of various Multi Unit Spectroscopic Explorer (MUSE) Guaranteed Time Observations (GTO). We also include a compilation of spectroscopic $\text{Ly}\alpha$ data from the literature spanning a wide redshift range ($z \approx 0 - 8$). First, restricting our analysis to double-peaked $\text{Ly}\alpha$ spectra, we find a tight correlation between the velocity offset of the red peak with respect to the systemic redshift, $V_{\text{peak}}^{\text{red}}$, and the separation of the peaks. Secondly, we find a correlation between $V_{\text{peak}}^{\text{red}}$ and the full width at half maximum of the $\text{Ly}\alpha$ line. Fitting formulas, to estimate systemic redshifts of galaxies with an accuracy of $\leq 100 \text{ km s}^{-1}$ when only the $\text{Ly}\alpha$ emission line is available, are given for the two methods.

Key words: ultraviolet : galaxies – galaxies : statistics – galaxies : starburst – galaxies : high-redshift

1 INTRODUCTION

In the last few decades, large samples of high-redshift galaxies ($z > 2$) have been assembled from deep photometric surveys based on broad/narrow-band selection techniques

*. E-mail: anne.verhamme@unige.ch

(Steidel et al. 2003; Ouchi et al. 2008; Bouwens et al. 2015; Finkelstein et al. 2015; Sobral et al. 2017, and references therein). In parallel, blind spectroscopic searches commonly rely on the Ly α line redshifted to the optical or the near-infrared to identify or confirm sources at $z \geq 2$ (e.g. Blanc et al. 2011; Bielby et al. 2011; Le Fèvre et al. 2015). The number of spectroscopic detections of Lyman Alpha Emitters (LAE) is now being increased dramatically with ongoing observational campaigns with the Multi Unit Spectroscopic Explorer (MUSE, Bacon et al. 2010) on ESO's VLT, allowing us to study galaxy formation and evolution with a homogeneous sample of sources over a large redshift range ($2.8 \lesssim z \lesssim 6.7$, e.g. Bacon et al. 2015, 2017; Drake et al. 2016; Herenz et al. 2017; Mahler et al. 2017; Caruana et al. 2018).

Several studies have demonstrated that the Ly α emission line is not exactly tracing systemic redshift (e.g. Shapley et al. 2003; Rakic et al. 2011; McLinden et al. 2011; Song et al. 2014; Hashimoto et al. 2015). Instead, the line profiles often show a complex structure which arguably originates from the propagation of resonant Ly α photons in neutral gas within the interstellar medium and/or in the vicinity of galaxies. Among the broad diversity of Ly α profiles in Ly α emitting galaxies, we identify the most common two categories : (i) spectra with a redshifted single peak ($\sim 2/3$ of Ly α emitting Lyman Break Galaxies, called LBGs, from Kulas et al. (2012)), and (ii) double-peaked profiles, with a prominent red peak and a smaller blue bump ($\sim 2/3$ of the remaining $1/3$ of Ly α emitting LBGs which are multiple peaked, from Kulas et al. (2012); 40% of the LAEs observed by Yamada et al. (2012)). We will refer to the latter as *blue bump LAEs* in the remainder of this paper. Understanding the nature of blue bump LAEs and studying their occurrence and evolution with redshift will be the goal of a forthcoming study. The vast majority of objects display a red peak shifted by a variable amount peaking around ~ 400 km s $^{-1}$ for Lyman Break Galaxies (LBGs, e.g. Shapley et al. 2003; Kulas et al. 2012), ~ 200 km s $^{-1}$ for LAEs (LAEs, e.g. Hashimoto et al. 2013; Song et al. 2014; Erb et al. 2014; Trainor et al. 2015; Henry et al. 2015; Hashimoto et al. 2015), and less than ~ 150 km s $^{-1}$ for a small sample of 5 local Lyman Continuum Emitters (Verhamme et al. 2017).

If not accounted for, this offset with respect to the systemic redshift can be problematic when addressing astrophysical issues which require accurate systemic redshift measurements (e.g. galaxy interactions, gas kinematics, baryonic acoustic oscillations, IGM-galaxy emission/absorption correlations). The scope of this paper is to investigate whether the Ly α profile shape can be used to determine the systemic redshift of galaxies. The outline of this Letter is as follows : in Sect.2, we gather recent spectroscopic data from MUSE GTO surveys and from the literature that have sufficient spectral resolution to investigate the Ly α line properties, as well as reliable systemic redshift measurements. In Sect. 3, We present two diagnostics which can be used to recover the systemic redshift from Ly α , that we compare to models in Sect.4. Sect.5 summarizes our findings.

2 A SAMPLE OF LAES WITH KNOWN SYSTEMIC REDSHIFT

In order to investigate the link between the shape of the Ly α line and the systemic redshift, we collect a diverse sample of LAEs with a precise measure of the systemic redshift. Our sample consists of high-redshift ($z > 2$) LAEs with detected C III] $\lambda\lambda$ 1907, 1909, [O III] $\lambda\lambda$ 4959, 5007 or H α λ 6563 emission, and low redshift ($z < 0.4$) LAEs with Ly α observations in the UV rest-frame obtained with the Cosmic Origins Spectrograph onboard *HST*, and ancillary optical spectra from the SDSS database containing several nebular emission lines from which the redshift is determined with great accuracy. We present these data in the following paragraphs. For each Ly α spectrum, we measure $V_{\text{peak}}^{\text{red}}$ as the location of the maximum of the Ly α flux redwards of the systemic redshift, and FWHM as the width of the part of the spectrum *uncorrected for instrumental broadening* with flux above half of the maximum, both directly on the data, without any modeling.

2.1 LAEs from MUSE GTO data

Stark et al. (2014) reported the detection of C III] $\lambda\lambda$ 1907, 1909 emission from low mass star-forming galaxies. When observed, this doublet is the strongest UV emission line after Ly α , and, in contrast to Ly α , it is an optically thin nebular line, tracing the systemic redshift¹ of the Ly α production site. The redshift window where Ly α and C III] are both observable within the VLT/MUSE spectral range is $2.9 < z < 3.8$. MUSE is an optical Integral Field Unit (IFU) spectrograph with medium spectral resolution (from $R \sim 2000$ in the blue to $R \sim 4000$ in the red).

Within several projects in the MUSE consortium using Guaranteed Time Observations (GTO, Bacon et al. 2017; Inami et al. 2017; Brinchmann et al. 2017; Maseda et al. 2017; Herenz et al. 2017; Mahler et al. 2017; Caruana et al. 2018) and Science Verification (SV) or commissioning data (Patrício et al. 2016), we find 13 LAEs with reliable C III] detections, that is, non contaminated by sky lines and with a S/N > 3 . We list these objects in Table 1 (see Maseda et al. 2017, for a systematic study of C III] emitters in the MUSE GTO data from the Hubble Ultra Deep Field). For each of these LAEs we measure the shift of the Ly α emission compared to C III], $V_{\text{peak}}^{\text{red}}$, the observed FWHM, and the separation of the Ly α peaks for the 8 blue bump LAEs among them.

2.2 High- z data from the literature

Stark et al. (2017) reported the detection of C III] from one of the highest redshift Ly α emitters ever observed ($z \sim 7.730$) with $V_{\text{peak}}^{\text{red}} \sim 340$ km s $^{-1}$; the Ly α FWHM = 360_{-70}^{+90} km s $^{-1}$ is measured by Oesch et al. (2015). Vanzella et al. (2016) report a narrow Ly α line observed at medium spectral resolution using VLT-Xshooter of a magnified star-forming galaxy at $z = 3.1169$, with $V_{\text{peak}}^{\text{red}}(\text{Ly}\alpha) \sim 100$ km s $^{-1}$ and

¹ C III] can be used as a redshift indicator when the two components of the doublet are well resolved, i.e. when $R \sim 2000$, because their relative strength depends on the density.

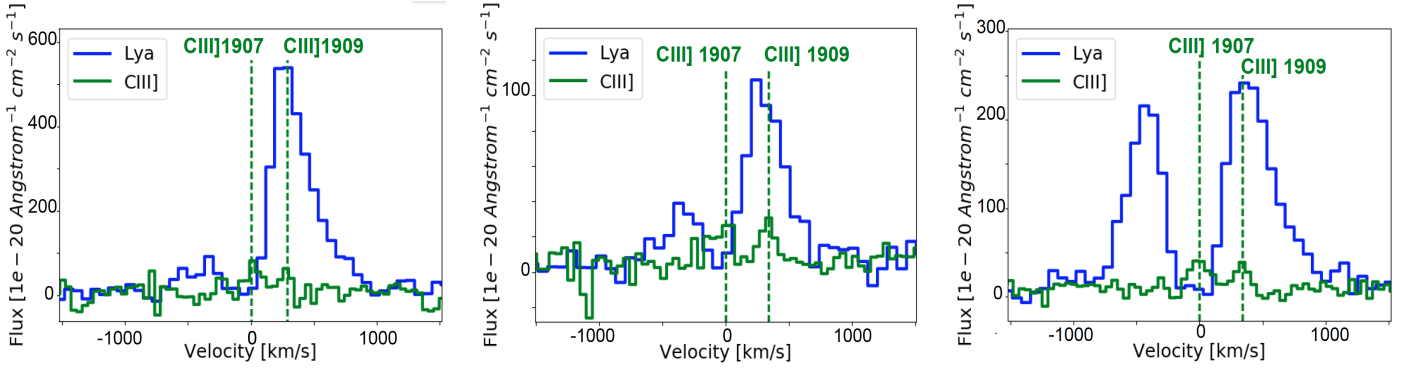


Figure 1. Three examples of rest-frame spectra of LAEs with detected C III] $\lambda\lambda$ 1907, 1909 doublet probing the systemic redshift in the MUSE-GTO observations. In each panel, the velocity shifts of the Ly α line are shown relative to C III] λ 1907Å. For all blue bump LAEs in our sample the systemic redshift falls in between the blue and red peaks of the Ly α emission.

$\text{FWHM}(\text{Ly}\alpha) \sim 104 \text{ km s}^{-1}$. From Hashimoto et al. (2015, 2017), we select the 6 LAEs observed with MagE ($R \sim 4100$). Their systemic redshifts have been obtained with either H α or [O III] lines. Three of these objects are blue-bump LAEs, for which we also measure the separation of the peaks. Kulas et al. (2012) reported that a significant fraction ($\sim 30\%$) of their Ly α emitting LBGs show a complex Ly α profile, with at least one secondary peak. Blue bump objects (their Group I) represent the majority of their profiles (11 out of 18 objects). We add these 11 objects to our sample of blue bumps LAEs.

2.3 Low- z data from the literature

Green Pea galaxies (hereafter GPs) are LAEs in the local Universe ($z \sim 0.1$ to 0.3 ; Jaskot & Oey 2014; Henry et al. 2015; Verhamme et al. 2017; Yang et al. 2017). The systemic redshift of these objects was compiled from the several nebular lines contained in their SDSS optical spectrum (e.g. Izotov et al. 2011). Note that the C III] emission line is out of the UV spectral range probed by the available *HST*-COS observations. For a sample of 17 GPs from Jaskot & Oey (2014); Henry et al. (2015); Verhamme et al. (2017), we measure $V_{\text{peak}}^{\text{red}}$ and FWHM on the data. For 21 new GP observations, we use the $V_{\text{peak}}^{\text{red}}$ and FWHM values computed by Yang et al. (2017) given in their Table 2. GPs nearly always exhibit blue bump Ly α profiles (Jaskot & Oey 2014; Henry et al. 2015; Verhamme et al. 2017). For the blue bump GPs, we also measure the separation of the peaks.

3 DERIVING SYSTEMIC REDSHIFT FROM LYMAN-ALPHA

3.1 Method 1 : systemic redshift of blue bump LAEs

In this section, only *blue bump spectra*, i.e. double peaks with a red peak higher than the blue peak, are considered. We note that, for all blue bump LAEs studied here, the systemic redshift always falls in-between the Ly α peaks, as illustrated in Fig 1 for three blue-bump MUSE Ly α +C III] emitters (see also Kulas et al. 2012; Erb et al. 2014; Yang et al. 2016). Fig. 2, left panel, shows a positive empirical

correlation between $V_{\text{peak}}^{\text{red}}$ and half of the separation of the peaks, $\Delta V_{1/2}$, for blue bump LAEs with known systemic redshift. We fit the data using the LTS_LINEFIT program described in Cappellari et al. (2013), which combines the Least Trimmed Squares robust technique of Rousseeuw & van Driessen (2006) into a least-squares fitting algorithm which allows for errors in both variables and intrinsic scatter². The best fit, shown by the red line on Fig. 2, is given by :

$$V_{\text{peak}}^{\text{red}} = 1.05(\pm 0.11) \times \Delta V_{1/2} - 12(\pm 37) \text{ km.s}^{-1} \quad (1)$$

This relation is so close to the one-to-one relation that we assume from now that the underlying "true" relation between $V_{\text{peak}}^{\text{red}}$ and $\Delta V_{1/2}$ is one-to-one, as expected from radiation transfer modeling (see Sect.4 below). The intrinsic scatter estimated from the linear regression is $53(\pm 9) \text{ km s}^{-1}$.

3.2 Method 2 : an empirical correlation between FWHM and systemic redshift

In this section, both single and double peaked profiles are considered. The measurements are always done on the red peak, and the red peak only. In the right panel of Fig. 2 we plot $V_{\text{peak}}^{\text{red}}$ versus FWHM for the full sample of LAEs presented in Sect. 2 (new MUSE LAEs measurements are reported in Table 1). There is a correlation between $V_{\text{peak}}^{\text{red}}$ and FWHM although less significant than for Method 1 (see the Pearson coefficients on each panel of Fig 2). We use the same method (Cappellari et al. 2013) to determine the empirical relation, which can be used to retrieve the systemic redshift of a galaxy :

$$V_{\text{peak}}^{\text{red}} = 0.9(\pm 0.14) \times \text{FWHM}(\text{Ly}\alpha) - 34(\pm 60) \text{ km.s}^{-1} \quad (2)$$

This relation is also compatible with the one-to-one relation, given the uncertainties in the fit parameters. The intrinsic scatter estimated from the linear regression is $72(\pm 12) \text{ km s}^{-1}$, slightly larger than with method 1.

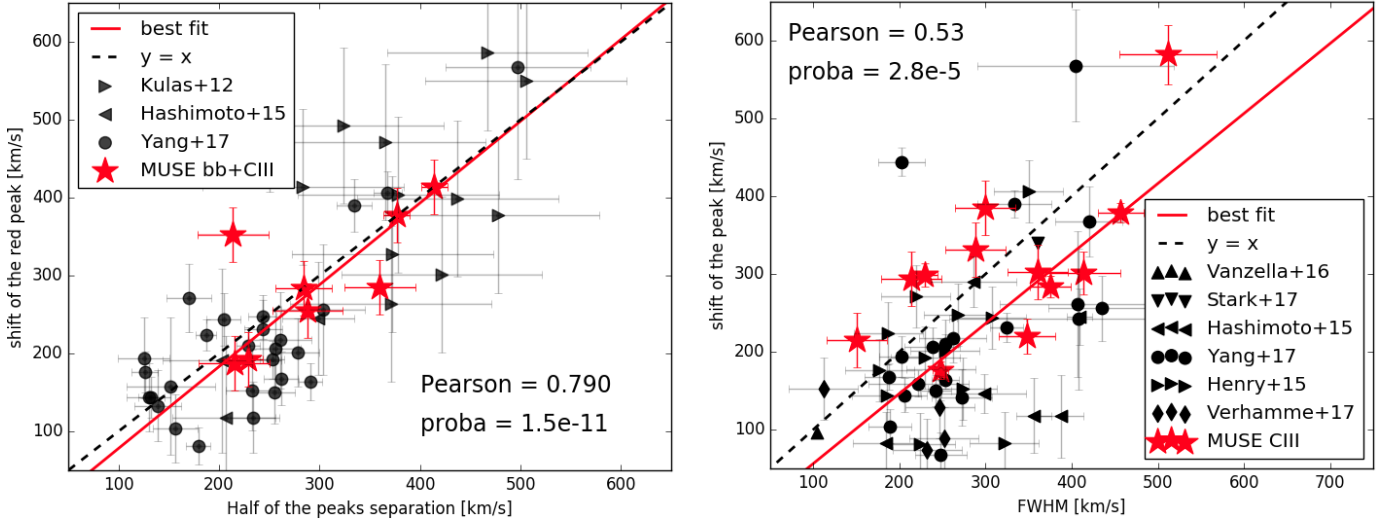


Figure 2. Empirical relations to determine systemic redshift from the shape of the Ly α emission. **Left** : correlation between the shift of the Ly α red peak, ($V_{\text{peak}}^{\text{red}}$) and half of the separation of the peaks ($\Delta V_{1/2}$) for a sample of LAEs with a known systemic redshift : 7 Ly α +C III] emitters with blue bump Ly α spectra from the MUSE GTO data (red stars), blue bump LAEs among the Yang et al. (2017) GP sample (black dots), blue bump LAEs among the Hashimoto et al. (2015) MagE sample and Group I LBGs from Kulas et al. (2012) (black triangles). **Right** : correlation between $V_{\text{peak}}^{\text{red}}$ and FWHM among Ly α + C III], H α or [O III] emitters. The black dashed line is the one-to-one relation. We checked that the correlation remains even discarding the two most upper left points. On both sides, the red curve is our best fit to the data, described by Eqs. (1) and (2). The Pearson coefficient and the probability of the null hypothesis are shown on each panel.

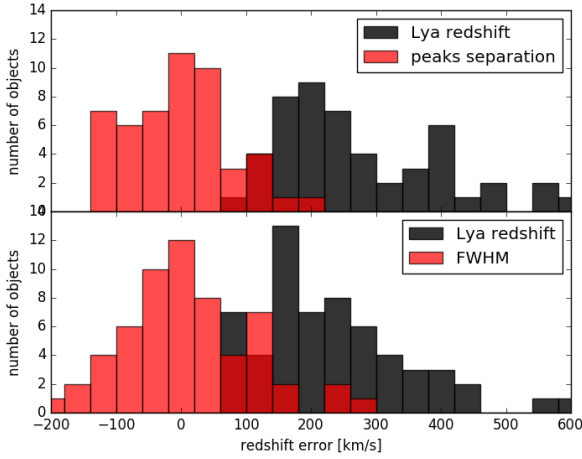


Figure 3. Comparison of the distributions of Ly α redshift errors ($= z_{\text{Ly}\alpha} - z_{\text{sys}}$, in black) with redshift distributions corrected with method 1 (in red, top panel) and with method 2 (in red, bottom panel).

3.3 Comparison of the methods

We check that the corrected redshifts from both methods give results that are closer to the systemic redshift of the objects than the “Ly α redshifts”, i.e. taking $V_{\text{peak}}^{\text{red}}$ as the systemic redshift, as usually done (Fig 3). The standard deviation of the red histograms (corrected redshifts), reflecting

both the intrinsic scatter and measurement errors, are comparable for the two methods, though slightly better for the blue bump method. We therefore propose to use half of the separation of the peaks as a proxy for the red peak shift of blue bump LAEs, and the Ly α FWHM for single peaked spectra³. They allow to recover the systemic redshift from the Ly α line, with an uncertainty lower than $\pm 100 \text{ km s}^{-1}$ from $z \approx 0$ to 7. This suggests that the same scattering processes, linking the line shift and the line width, are at play at every redshift, and that the effect of the IGM does not erase this correlation.

4 DISCUSSION

4.1 Effect of the spectral resolution

These two methods to retrieve the systemic redshift of a LAE from the shape of its Ly α profile rely on measurements of either the positions of the blue and red Ly α emission peaks or the (red peak) FWHM. Both of these measures are affected by the spectral resolution. Although the data points presented in Sect 3. were collected from the literature and MUSE surveys and span a range of spectral resolutions from $R \sim 1000$ (LRIS) to $R \sim 5000$ (X-Shooter, *HST*-COS), they all seem to follow the same relation.

We investigated the effect of spectral resolution on synthetic spectra constructed from Ly α radiation transfer simulations. Poorer spectral resolution broadens the peaks, and since Ly α profiles are often asymmetric, it also has the effect of shifting the peak towards longer wavelengths. The latter

³ We have also tested the relation between Ly α EWs and $V_{\text{peak}}^{\text{red}}$, but did not find any significant correlation.

² <http://www-astro.physics.ox.ac.uk/~mxc/software/#lts>

effect is weaker than the broadening. As a consequence, the effect of spectral resolution may flatten the slope but seems not to break the correlation.

4.2 Comparison with models

We now compare our results with numerical simulations of Ly α radiative transfer in expanding shells performed with the MCLy α code (Schaerer et al. 2011; Verhamme et al. 2006). These models describe in a simple, idealized, way the propagation of Ly α photons emitted in HII regions through gas outflows which seem ubiquitous in star-forming galaxies, especially at high redshift (Shapley et al. 2003; Steidel et al. 2010; Hashimoto et al. 2015). Assuming a central point-source surrounded by an expanding shell of gas with varying HI column density (N_{HI}), speed (V_{exp}), dust opacity (τ_{d}) and temperature (described by the Doppler parameter $b \propto \sqrt{T}$), shell models have proven very successful in reproducing a large diversity of Ly α line profiles. Here, we use simulations with different intrinsic Gaussian line widths (σ_i) and various shell parameter values (N_{HI} , V_{exp} , τ_{d} , b), degraded to mimic the MUSE spectral resolution. We measure FWHM, $V_{\text{peak}}^{\text{red}}$ and $\Delta V_{1/2}$ the same way as for the data.

We compare the observed correlation between $V_{\text{peak}}^{\text{red}}$ and the separation between the peaks of blue-bump LAEs ($\Delta V_{1/2}$) with results from models that produce double-peak profiles (Fig. 4, left panel). Predictions from expanding shell models lie very close to the one-to-one relation and reproduce nicely the observed properties of the Ly α lines. Objects with increasing $V_{\text{peak}}^{\text{red}}$ and $\Delta V_{1/2}$ correspond to expanding shells with larger HI column densities. This echoes the analytical solutions for Ly α RT in static homogeneous media (Neufeld 1990; Dijkstra et al. 2006) that yield profiles with symmetric peaks around the line centre, whose positions are primarily set by the HI opacity and correspond to $V_{\text{peak}}^{\text{red}} \propto \tau_{\text{HI}}^{1/3}$.

As shown in Fig. 4 (right panel), the correlation between the shift of the red peak and the FWHM of the Ly α line naturally arises from scattering processes. The slope predicted by the models is close to one whereas the relation derived from observations in Section 3 is shallower (≈ 0.9 ; red curve in the right panel of Figs. 2,4). However, it is worth pointing out that we explore a much larger range of FWHMs in the right panel of Fig. 4 (from 0 to 1200 km s $^{-1}$) compared to Fig. 2 where observed FWHMs vary from 214 to 512 km s $^{-1}$. For FWHM values less than 600 km s $^{-1}$, the model predictions lie close to the FWHM- $V_{\text{peak}}^{\text{red}}$ relation derived in Section 3. Although the exact location of each simulated object in the FWHM- $V_{\text{peak}}^{\text{red}}$ plane seems to depend on each parameter, we see that models with higher HI column densities lead to broader lines and larger shifts of the peak (color-coded circles). A similar trend is found by Zheng & Wallace (2014) who performed Ly α radiation transfer simulations in anisotropic configurations (bipolar outflows) and inhomogeneous media (i.e. HI distributions with velocity or density gradients). Overall, this may suggest that the FWHM- $V_{\text{peak}}^{\text{red}}$ correlation holds regardless of the assumed geometry and kinematics of the outflows, and that the HI opacity of the ISM and/or the medium surrounding galaxies (i.e. the CGM) is the main driver that shapes the observed Ly α line profiles.

5 CONCLUSIONS

The recent increase in the number of LAEs with detected nebular lines allows to calibrate empirical methods to retrieve the systemic redshift from the shape of the Ly α line. In addition to measurements from the literature, we report 13 new detections from several MUSE GTO programs. We searched for Ly α +CIII] emitters in the MUSE-Deep survey (Bacon et al. 2017), behind $z \sim 0.7$ galaxy groups (Contini et al, in prep), and lensed by three clusters (SMACSJ2031.8-4036 in Patrício et al. 2016, AS1063, MACS0416 in Richard et al, in prep).

We find a robust correlation between the shift of the Ly α peak with respect to systemic redshift ($V_{\text{peak}}^{\text{red}}$) and half of the separation of the peaks ($\Delta V_{1/2}$) for LAEs with blue bump spectra. The intrinsic scatter around the relation is ± 53 km s $^{-1}$. We also find a correlation between the shift of the Ly α peak with respect to systemic redshift ($V_{\text{peak}}^{\text{red}}$) and its width at half-maximum (FWHM), for LAEs with known systemic redshift. The intrinsic scatter is of the same order (± 73 km s $^{-1}$). These two relations have been approximated by linear fitting formulas as given in Eq (1) and (2). These formulae have been derived for data with spectral resolution $1000 < R < 5000$, they should be used on data with similar spectral resolution.

The relative redshift error if estimated from Ly α with $V_{\text{peak}}^{\text{red}} = 300$ km s $^{-1}$ is $(\Delta z / z)(\text{Ly}\alpha) = ((1+z) \times (V_{\text{peak}}^{\text{red}} / c)) / z \sim 10^{-3}$ at $z = 3$. The two methods presented in this letter can therefore help reduce systematic errors on distance measures. This is of great importance for redshift surveys at $z \gtrsim 3$, where spectroscopic redshifts often rely on the Ly α emission line. Futures observations with better spectral resolution should allow to refine the proposed relations.

ACKNOWLEDGEMENTS

We thank the anonymous referee for her/his helpful report. AV is supported by a Marie Heim Vögtlin fellowship of the Swiss National Foundation. TG is grateful to the LABEX Lyon Institute of Origins (ANR-10-LABX-0066) of the Université de Lyon for its financial support within the program "Investissements d'Avenir" (ANR-11-IDEX-0007) of the French government operated by the National Research Agency (ANR). TC, EV, JZ acknowledge support of the ANR FOGHAR (ANR-13-BS05-0010-02), the OCEVU Labex (ANR-11-LABX-0060) and the A*MIDEX project (ANR-11-IDEX-0001-02) funded by the "Investissements d'Avenir" French government program managed by the ANR. RB and FL acknowledges support from the ERC advanced grant 339659-MUSICOS. JR and VP acknowledge support from the ERC starting grant 336736-CALENDS. RAM acknowledges support by the Swiss National Science Foundation. JS acknowledges support from the ERC grant 278594-GasAroundGalaxies. JB acknowledges support by Fundação para a Ciência e a Tecnologia (FCT) through national funds (UID/FIS/04434/2013) and by FEDER through COMPETE2020 (POCI-01-0145-FEDER-007672) and Investigador FCT contract IF/01654/2014/CP1215/CT0003.

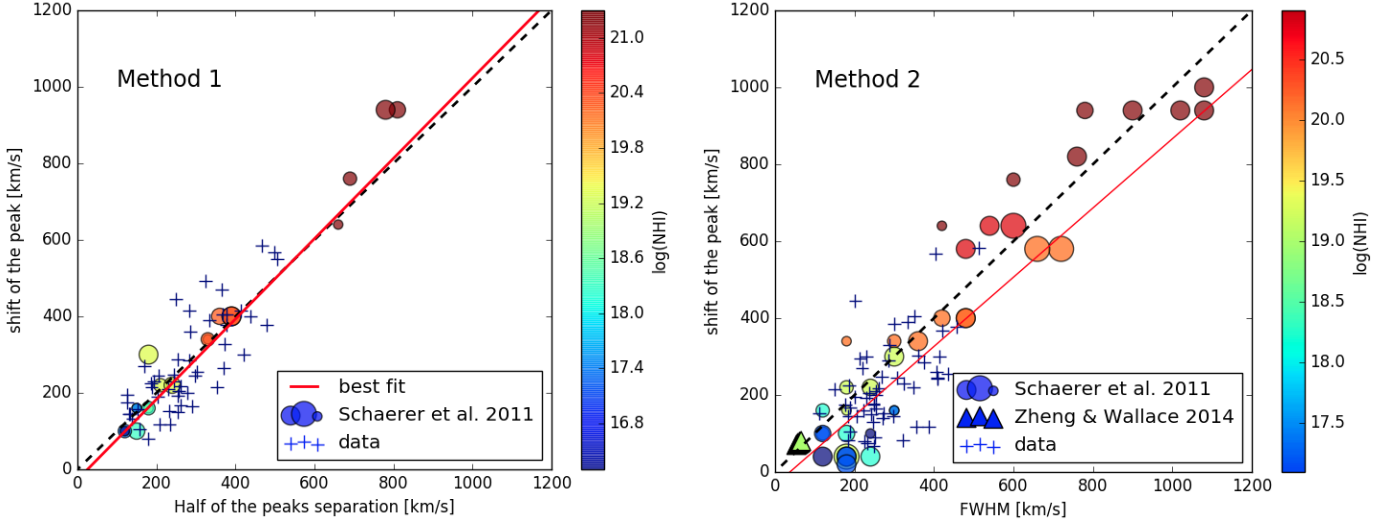


Figure 4. Points show the relationship between half of the separation of the peaks and the shift of the Ly α line, and between the FWHM and the shift of the Ly α line, for synthetic spectra from expanding shells, spheres or bi-conical outflows (Schaerer et al. 2011; Zheng & Wallace 2014). The trend is driven by the column density of the scattering medium, but holds for the different idealized geometries. The symbol colors scale with the column density (in cm^{-2}) of the shells and symbol sizes scale with the radial expansion velocity (from 0 to 400 km s^{-1}). The red line and dashed black line are identical as in Fig 2.

Références

- Bacon R., et al., 2010, in *Ground-based and Airborne Instrumentation for Astronomy III*. p. 773508, doi :10.1117/12.856027
- Bacon R., et al., 2015, *A&A*, 575, A75
- Bacon R., et al., 2017, preprint, ([arXiv:1710.03002](https://arxiv.org/abs/1710.03002))
- Bielby R. M., et al., 2011, *MNRAS*, 414, 2
- Blanc G. A., et al., 2011, *ApJ*, 736, 31
- Bouwens R. J., et al., 2015, *ApJ*, 803, 34
- Brinchmann J., et al., 2017, preprint, ([arXiv:1710.05062](https://arxiv.org/abs/1710.05062))
- Cappellari M., et al., 2013, *MNRAS*, 432, 1709
- Caruana J., et al., 2018, *MNRAS*, 473, 30
- Dijkstra M., Haiman Z., Spaans M., 2006, *ApJ*, 649, 14
- Drake A. B., et al., 2016, preprint, ([arXiv:1609.02920](https://arxiv.org/abs/1609.02920))
- Erb D. K., et al., 2014, *ApJ*, 795, 33
- Finkelstein S. L., et al., 2015, *ApJ*, 810, 71
- Hashimoto T., Ouchi M., Shimasaku K., Ono Y., Nakajima K., Rauch M., Lee J., Okamura S., 2013, *ApJ*, 765, 70
- Hashimoto T., et al., 2015, *ApJ*, 812, 157
- Hashimoto T., et al., 2017, *MNRAS*, 465, 1543
- Henry A., Scarlata C., Martin C. L., Erb D., 2015, *ApJ*, 809, 19
- Herenz E. C., et al., 2017, preprint, ([arXiv:1705.08215](https://arxiv.org/abs/1705.08215))
- Inami H., et al., 2017, preprint, ([arXiv:1710.03773](https://arxiv.org/abs/1710.03773))
- Izotov Y. I., Guseva N. G., Thuan T. X., 2011, *ApJ*, 728, 161
- Jaskot A. E., Oey M. S., 2014, *ApJ*, 791, L19
- Kulas K. R., Shapley A. E., Kollmeier J. A., Zheng Z., Steidel C. C., Hainline K. N., 2012, *ApJ*, 745, 33
- Le Fèvre O., et al., 2015, *A&A*, 576, A79
- Mahler G., et al., 2017, preprint, ([arXiv:1702.06962](https://arxiv.org/abs/1702.06962))
- Maseda M. V., et al., 2017, preprint, ([arXiv:1710.06432](https://arxiv.org/abs/1710.06432))
- McLinden E. M., et al., 2011, *ApJ*, 730, 136
- Neufeld D. A., 1990, *ApJ*, 350, 216
- Oesch P. A., et al., 2015, *ApJ*, 804, L30
- Ouchi M., et al., 2008, *ApJS*, 176, 301
- Patrício V., et al., 2016, *MNRAS*, 456, 4191
- Rakic O., Schaye J., Steidel C. C., Rudie G. C., 2011, *MNRAS*, 414, 3265
- Schaerer D., Hayes M., Verhamme A., Teyssier R., 2011, *A&A*, 531, A12
- Shapley A. E., Steidel C. C., Pettini M., Adelberger K. L., 2003, *ApJ*, 588, 65
- Sobral D., et al., 2017, *MNRAS*, 466, 1242
- Song M., et al., 2014, *ApJ*, 791, 3
- Stark D. P., et al., 2014, *MNRAS*, 445, 3200
- Stark D. P., et al., 2017, *MNRAS*, 464, 469
- Steidel C. C., Adelberger K. L., Shapley A. E., Pettini M., Dickinson M., Giavalisco M., 2003, *ApJ*, 592, 728
- Steidel C. C., Erb D. K., Shapley A. E., Pettini M., Reddy N., Bogosavljević M., Rudie G. C., Rakic O., 2010, *ApJ*, 717, 289
- Trainor R. F., Steidel C. C., Strom A. L., Rudie G. C., 2015, *ApJ*, 809, 89
- Vanzella E., et al., 2016, *ApJ*, 821, L27
- Verhamme A., Schaerer D., Maselli A., 2006, *A&A*, 460, 397
- Verhamme A., Orlicová I., Schaerer D., Izotov Y., Worseck G., Thuan T. X., Guseva N., 2017, *A&A*, 597, A13
- Yamada T., Matsuda Y., Kousai K., Hayashino T., Morimoto N., Umemura M., 2012, *ApJ*, 751, 29
- Yang H., Malhotra S., Gronke M., Rhoads J. E., Dijkstra M., Jaskot A., Zheng Z., Wang J., 2016, *ApJ*, 820, 130
- Yang H., et al., 2017, preprint, ([arXiv:1701.01857](https://arxiv.org/abs/1701.01857))
- Zheng Z., Wallace J., 2014, *ApJ*, 794, 116

This paper has been typeset from a $\text{\TeX}/\text{\LaTeX}$ file prepared by the author.

Table 1. MUSE $\text{Ly}\alpha+\text{CIII}]$ emitters. The 6th column indicates the separation of the peaks (i.e. $2\times\Delta V_{1/2}$, in km s^{-1}) for blue bump LAEs, and is left empty for single-peaked profiles. a : Patricio et al. 2016; b : Richard et al. 2018 in prep; c : Bacon et al. 2017, Inami et al. 2017, Maseda et al. 2017; d : Contini et al. 2018 in prep.

ID	RA	DEC	EW [\AA]	$V_{\text{peak}}^{\text{red}}$ [km s^{-1}]	FWHM [km s^{-1}]	ΔV [km s^{-1}]	$z_{\text{sys, CIII}}$	observations
sys 1 ^a	307.97040	-40.625694	32	176 ± 11	248 ± 9	–	3.5062	commissioning
mul 11 ^b	342.175042	-44.541031	222	215 ± 35	150 ± 35	375 ± 35	3.1163	AS1063
mul 14 ^b	342.178833	-44.535869	29	385 ± 35	300 ± 35	–	3.1150	AS1063
sys 44 ^b	64.0415559	-24.0599916	57	303 ± 35	360 ± 35	570 ± 35	3.2886	MACS0416
sys 132 ^b	64.0400838	-24.0667408	62	331 ± 35	288 ± 35	510 ± 35	3.2882	MACS0416
106 ^c	53.163726	-27.7790755	72	379 ± 13	414 ± 13	828 ± 35	3.2767	udf-10
118 ^c	53.157088	-27.7802688	65	301 ± 28	284 ± 28	568 ± 35	3.0173	udf-10
1180 ^c	53.195735	-27.7827171	80	220 ± 23	348 ± 32	–	3.3228	udf mosaic
6298 ^c	53.169249	-27.7812550	83	582 ± 38	512 ± 56	–	3.1287	udf-10
6666 ^c	53.159576	-27.7767193	52	284 ± 13	377 ± 11	754 ± 35	3.4349	udf-10
50 ^d	150.149656	2.061272	50	431 ± 42	268 ± 39	–	3.8237	GR30
48 ^d	149.852989	2.488099	68	294 ± 35	214 ± 35	705 ± 35	3.3280	GR34
102 ^d	150.050268	2.600025	76	299 ± 15	229 ± 15	385 ± 35	3.0400	GR84